Metal-Centered 17-Electron Radicals CpM(CO)(3) (center dot) (M = Cr, Mo, W): A Combined Negative Ion Photoelectron Spectroscopic and Theoretical Study

ARTICLE *in* ORGANOMETALLICS · MARCH 2013

Impact Factor: 4.13 · DOI: 10.1021/om3011454

7 AUTHORS, INCLUDING:

Gao-Lei Hou
Pacific Northwest National Laboratory
39 PUBLICATIONS **56** CITATIONS
SEE PROFILE

Xue-Bin Wang
Pacific Northwest National Laboratory
192 PUBLICATIONS **5,230** CITATIONS
SEE PROFILE

ORGANOMETALLICS

Article

pubs.acs.org/Organometallics

Metal-Centered 17-Electron Radicals $CpM(CO)_3^{\bullet}$ (M = Cr, Mo, W): A Combined Negative Ion Photoelectron Spectroscopic and Theoretical Study

Edwin F. van der Eide,[†] Gao-Lei Hou,[‡,§] S. H. M. Deng,[†] Hui Wen,[†,§] Ping Yang,*[,‡] R. Morris Bullock,*[,†] and Xue-Bin Wang*[,†]

[†]Chemical and Materials Sciences Division and [‡]Environmental Molecular Sciences Laboratory, Pacific Northwest National Laboratory, P.O. Box 999, Richland, Washington 99352, United States

Supporting Information

ABSTRACT: Despite the importance of group 6 metal-centered 17-electron radicals $CpM(CO)_3^{\bullet}$ (M = Cr, Mo, W) in establishing many of the fundamental reactions now known for metal-centered radicals, spectroscopic characterization of their electronic properties and structures has been very challenging, due to their high reactivity. Here we report a gas-phase study of these species by photodetachment photoelectron spectroscopy (PES) of their corresponding 18-electron anions and by theoretical electronic structure calculations. Three well-separated spectral features are observed by PES for each anionic species. Electron affinities (EAs) of $CpM(CO)_3^{\bullet}$ were experimentally measured from the threshold of each spectrum and were found to be 2.38 ± 0.02 (M = Cr), 2.63 ± 0.02 (Mo), and 2.63 ± 0.01 eV (W). These experimental values correlate well with the reported redox potentials measured in solution. Theoretical calculations for all anionic and neutral (radical) species gave calculated EAs and band gaps that are in good agreement with the experimental data. Molecular orbital (MO) analyses for each anion indicate that the *top three* occupied MOs are mainly metal-based and contribute to the first spectral feature, whereas the *next two* MOs are associated with Cp−M π bonding and contribute to the second spectral feature. The calculations further exhibit appreciable anion-to-neutral structural changes for all three species, with the change for the W species being the smallest.

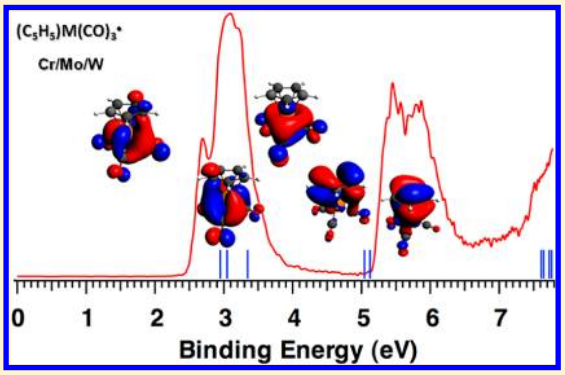

INTRODUCTION

The existence of 17-electron organometallic radicals has long been established.[1,2] Their high reactivity and intermediacy in fundamental organometallic reactions has spurred extensive interest in metal-centered radicals over several decades.[3−14] Group 6 metal centered $CpM(CO)_3^{\bullet}$ (Cp = η^5-C_5H_5; M = Cr, Mo, W) radicals with a three-legged piano-stool geometry are among the well-known examples of metal-centered radicals. Because of the rapid self-dimerization of these radicals (essentially irreversible for Mo and W,[4−6] $k_{dim} \approx (3–6) \times 10^9$ M^{-1} s^{-1}, and reversible for Cr,[7] $k_{dim} \approx 3 \times 10^8$ M^{-1} s^{-1}), they are difficult to study under ambient conditions. For the Mo and W radicals, infrared spectroscopic characterization of the radicals has resulted from elegant flash photolysis studies;[12] the Cr derivative has additionally been characterized by ^{1}H NMR[15] and EPR[16] spectroscopy. Solution electrochemical measurements on the stable 18e anions $CpM(CO)_3^-$ have provided the potentials for the 17e/18e couples $[CpM(CO)_3]^{\bullet/-}$.[17] Ligand steric effects have been explored to improve the stability of these 17e radicals by substitution of a CO with a bulky phosphine ligand[16,18] or an *N*-heterocyclic carbene ligand.[19]

Despite the interest in them, there has been no systematic *experimental* study on the electronic structures of the 17e organometallic radicals $CpM(CO)_3^{\bullet}$. Our knowledge about their electronic structures and chemical bonding has instead largely come from theoretical investigations using the Hartree−Fock method[16] and extended Hückel molecular orbital and fragment analysis.[20−22] Information about radical cations isolobal with neutral group 6 radicals $CpM(CO)_3^{\bullet}$, e.g. $[(benzene)M(CO)_3]^{\bullet+}$ (M = Cr, Mo, W) and $[CpMn(CO)_3]^{\bullet+}$, has been obtained by photoionization of the respective neutral 18e complexes,[23−25] and MO schemes for these compounds have been derived.[22−25]

Negative ion photodetachment photoelectron spectroscopy (PES) coupled with electrospray ionization (ESI) is a technique ideally suited for probing chemical bonding and electronic structures of metal complexes. Such experiments induce transitions from the ground state of the anion to the ground and excited states of the corresponding neutral radical, directly yielding electronic structure information for the neutral radical,[26] as well as its electron affinity. Many negatively

Received: November 26, 2012
Published: March 25, 2013

   dx.doi.org/10.1021/om3011454 | *Organometallics* 2013, 32, 2084−2091

charged inorganic and organometallic species existing in the solution phase (often closed-shell species) can be transferred to the gas phase by ESI, enabling the electronic structures of these solution-phase species to be studied in the gas phase. This experimental method, in combination with high-level theoretical calculations, has been previously shown to be a powerful approach to probe the electronic structures and bonding properties of isolated metal complexes without complications that can arise in the condensed phase.[27,28] For example, the dimerization of $CpM(CO)_3^{\bullet}$ that affects measurements in solution[17] is not an issue in ESI-PES, where only very low concentrations (typically 10^3–10^4 anions/cm^3) of the anion are required.

In this paper, we report a synergistic low-temperature PES and theoretical study of $CpM(CO)_3$ anions and radicals. The 18e $[CpM(CO)_3]^-$ anions were readily obtained in the gas phase by ESI, and their photoelectron spectra were recorded at several different photon energies (355, 266, 193, and 157 nm). The electron affinities (EAs) of $CpM(CO)_3^{\bullet}$ as determined here from the threshold of each anion's spectrum are in good agreement with solution-phase redox potentials for these complexes[17] but do not correlate with the previously reported EAs of the 12e $M(CO)_3$ systems,[29] presumably because of the significant electronic influence of the Cp ligand. Density functional theory (DFT) calculations were performed on the anions and corresponding neutral radicals to interpret the observed spectral features and bonding nature of these highly reactive 17e radicals.

EXPERIMENTAL DETAILS

General Considerations. Synthetic manipulations were carried out under N_2 using standard Schlenk and inert-atmosphere glovebox techniques. Acetonitrile, diethyl ether, hexanes, and tetrahydrofuran were purified by passage through neutral alumina, using an Innovative Technology, Inc., Pure Solv solvent purification system. CD_3CN was dried over P_2O_5 and vacuum-distilled through a glass wool plug. $[CpCr(CO)_3]_2$,[30a] $Mo(CO)_3(MeCN)_3$,[30b] NaCp·DME,[30c] and $Na^+[CpW(CO)_3]^-$ [30d] were prepared as described in the literature. 18-crown-6 was used as received. NMR spectra were recorded on a Varian spectrometer (500 MHz for ^{1}H); spectra were referenced relative to the NMR solvent (^{1}H, δ 1.94 for CHD_2CN; ^{13}C, δ 1.3 for CD_3CN). Solution IR spectra were recorded using a Nicolet iS10 FTIR spectrometer with demountable sealed-liquid CaF_2 cells (International Crystal Laboratories). Elemental analyses were performed by Atlantic Microlab (Norcross, GA).

Synthesis of [Na(18-crown-6)]$^+$[CpCr(CO)$_3$]$^-$. $[CpCr(CO)_3]_2$ (0.150 g, 0.373 mmol) and Na metal (40 mg, 1.7 mmol) were placed in a vial. THF (3 mL) was added, and the very dark green solution was stirred for 1 h, during which time the color changed to yellow-brown. IR spectroscopy (THF solution, $\tilde{\nu}_{CO}$ 1897, 1794, 1742 cm^{-1}) indicated that conversion to $Na^+[CpCr(CO)_3]^-$ was clean and complete. The solution was filtered and added to a solution of 18-crown-6 (0.208 g, 0.789 mmol) in 0.5 mL of THF. The resulting yellow solution was layered with hexane (4 mL), and slow diffusion over 3 days gave yellow single crystals. The crystals were washed with Et_2O (3 × 4 mL), which caused them to disintegrate into microcrystals, which were dried under vacuum. Yield: 0.343 g (0.702 mmol, 94%). ^{1}H NMR (CD_3CN, 500 MHz, 298 K): δ 4.41 (s, 5H, Cp), 3.58 (s, 24H, 18-crown-6). $^{13}C\{^1H\}$ NMR (CD_3CN, 125 MHz, 298 K): δ 247.0 (s, Cr-CO), 82.7 (s, Cp), 70.1 (s, 18-crown-6). IR ($\tilde{\nu}_{CO}$, MeCN solution): 1893 (s), 1774 (br vs) cm^{-1}. Anal. Calcd for $C_{20}H_{29}NaO_9Cr$: C, 49.18; H, 5.98. Found: C, 49.15; H, 6.08.

Synthesis of [Na(18-crown-6)]$^+$[CpMo(CO)$_3$]$^-$. $Mo(CO)_3(MeCN)_3$ (0.205 g, 0.676 mmol) was suspended in THF (2 mL) and NaCp·DME (0.128 g, 0.712 mmol) was added as a solid, causing all of the solids to dissolve to give a yellow solution. IR spectroscopy after 1 h at room temperature (THF solution, $\tilde{\nu}_{CO}$ 1900, 1797, 1746 cm^{-1}) indicated that conversion to $Na^+[CpMo(CO)_3]^-$ was clean and complete. The solution was filtered and added to a solution of 18-crown-6 (0.198 g, 0.749 mmol) in THF (0.5 mL). The resulting yellow solution was layered with hexane (4 mL), and slow diffusion over 5 days gave light yellow crystals. The crystals were washed with Et_2O (3 × 4 mL) and dried under vacuum. Yield: 0.342 g (0.642 mmol, 95%). ^{1}H NMR (CD_3CN, 500 MHz, 298 K): δ 5.06 (s, 5H, Cp), 3.58 (s, 24H, 18-crown-6). $^{13}C\{^1H\}$ NMR (CD_3CN, 125 MHz, 298 K): δ 236.5 (s, Mo-CO), 87.1 (s, Cp), 70.1 (s, 18-crown-6). IR ($\tilde{\nu}_{CO}$, MeCN solution): 1897 (s), 1777 (br vs) cm^{-1}. Anal. Calcd for $C_{20}H_{29}NaO_9Mo$: C, 45.12; H, 5.49. Found: C, 45.28; H, 5.41.

Low-Temperature Photoelectron Spectroscopy. The PES experiments were performed using a low-temperature ESI source-PES apparatus, details of which have been reported.[31] The gaseous 18e anions, $CpM(CO)_3^-$ (M = Cr, Mo, W), were readily produced by spraying freshly prepared ~10^{-4} M acetonitrile solutions of $[Na(18\text{-crown-6}]^+[CpM(CO)_3]^-$ (M = Cr, Mo) and $Na^+[CpW(CO)_3]^-$. The anions produced by the ESI source were guided by two RF-only quadrupoles and a 90° quadrupole deflector into a cryogenically controlled ion trap, where they were accumulated and cooled by collisions with a buffer gas of ~0.1 mTorr (20% H_2, balance helium) for 20–80 ms, before being pulsed out into the extraction zone of a time-of-flight mass spectrometer with a 10 Hz repetition rate. The ion trap was operated at 20 K in the current experiments. The low temperature eliminates hot bands in the spectrum.

During each PES experiment, the desired anions were mass-selected and decelerated before being intercepted by a probe laser beam in the photodetachment zone of a magnetic bottle photoelectron analyzer. In the current study, four wavelengths were used: 355 nm (3.496 eV) and 266 nm (4.661 eV) from an Nd:YAG laser and 193 nm (6.424 eV) and 157 nm (7.867 eV) from an ArF and F_2 laser. All of the lasers were operated at a 20 Hz repetition rate with the ion beam off during alternating laser shots, permitting shot-by-shot background subtraction. Photoelectrons were collected at nearly 100% efficiency by the magnetic bottle and analyzed in a 5.2 m long electron flight tube. Time-of-flight photoelectron spectra were collected and converted to kinetic energy spectra, calibrated by the known spectra of I^-, $Cu(CN)_2^-$,[28] and ClO_2^-.[32] The electron binding energy spectra were obtained by subtracting the kinetic energy spectra from the detachment photon energies. The electron energy resolution was about 2%: i.e., ~20 meV for 1 eV electrons.

Theoretical Methods. First-principles calculations based on density functional theory were performed to study the geometries, electronic structures, and bonding properties of the 18e anions $CpM(CO)_3^-$ (M = Cr, Mo, W) and their corresponding 17e neutral radicals $CpM(CO)_3^{\bullet}$ using the spin-polarized generalized gradient approximation (GGA) with the Perdew–Burke–Ernzerhof (PBE) exchange-correlation functional[33] implemented in the Amsterdam Density Functional (ADF 2010.02) program.[34] Slater basis sets with quality of triple-ζ plus one polarization functions were used, with the frozen core approximation applied to $[1s^2–2p^6]$ for Cr, $[1s^2–3d^{10}]$ for Mo, $[1s^2–4d^{10}]$ for W, and $[1s^2]$ for O and C.[35] Scalar relativistic effects were taken into account by the zeroth-order regular approximation (ZORA) to the Dirac equation.[36] Geometries were optimized without symmetry constraints, and vibrational frequencies were computed to verify that the optimized geometries were energy minima and to interpret the observed vibrational progressions.[37] The orbital compositions were obtained by Mulliken population analysis of each particular molecular orbital. The populations of the metal d orbitals of each complex are given in Table 3.

For each $CpM(CO)_3^-$ system, the adiabatic detachment energy (ADE), equivalent to the EA of the neutral radical, was calculated as the energy difference between the ground state of the anion and the ground state of the neutral radical species from which an electron has been removed from the HOMO of the anion, including zero-point energy (ZPE) corrections. The structures of the 18e anion and the 17e radical were both at their respective optimized geometries. The first vertical detachment energy (VDE_{HOMO}) for this same electron was obtained as the energy difference between the ground-state energy of

dx.doi.org/10.1021/om3011454 | Organometallics 2013, 32, 2084–2091

the anion and the energy of the neutral radical at the structure of the anion. To determine the higher VDE for an electron in an MO below the HOMO, the energy to promote the electron into the hole created upon the ejection of the electron from the HOMO of the anion was calculated and then summed with VDE_{HOMO}. The time-dependent density functional theory (TDDFT) approach[38] was used to calculate these transition energies for the neutral radical at the anion geometry. This approach has previously been applied to photoelectron spectra and showed good agreement with experimental measurements.[39,40]

EXPERIMENTAL RESULTS

Figure 1 shows photoelectron spectra of $CpCr(CO)_3^-$ at 20 K measured at 355, 266, and 157 nm. Only one broad band X

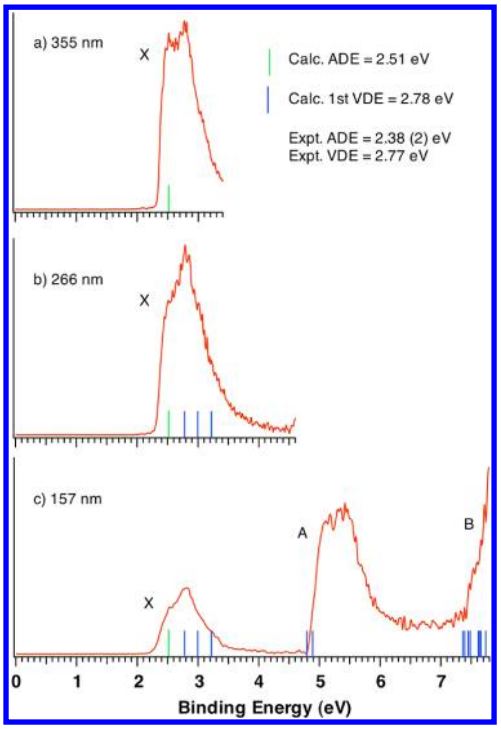

Figure 1. Low-temperature (20 K) photoelectron spectra of $CpCr(CO)_3^-$ at 355 (a), 266 (b), and 157 nm (c). The calculated adiabatic (ADE, green bar) and vertical detachment energies (VDEs, blue bars) are indicated.

(2.3 − 3.5 eV) was observed at both 355 and 266 nm, but with a different spectral envelope, suggesting that more than one electronic transition is involved. At 157 nm, one additional feature A (4.8−6.0 eV) and an onset of the third band B (>7.4 eV) were observed. The 157 nm spectrum clearly shows that the electronic states of $CpCr(CO)_3^{\bullet}$ are grouped, with significant band gaps in between. As no vibrational structures were resolved in the spectra, the ADE is estimated for $CpCr(CO)_3^-$ (corresponding to the EA of the neutral radical). This estimate was made by drawing a straight line along the rising edge of the ground state transition and adding the instrumental resolution (fwhm) to the crossing point with the binding energy axis to be 2.38 ± 0.02 eV (Table 1) from the 355 nm spectrum, which was also confirmed (within experimental uncertainty) from the 266 and 157 nm spectra. Further details are provided in the Supporting Information.

The photoelectron spectra of $CpMo(CO)_3^-$ at 20 K are shown in Figure 2. Similar spectral features were observed at 355 and 266 nm (X) and 157 nm (X, A, and B) in comparison to $CpCr(CO)_3^-$. A weak spectral feature at lower binding

Table 1. Observed and Calculated Adiabatic Detachment Energies (ADEs) for $CpM(CO)_3^-$ and Comparison with Electrochemical Potentials in Solution

	gas phase		MeCN solution
M	exptl ADE (eV)[a]	calcd ADE (eV)[b]	E° (V vs $Cp_2Fe^{+\bullet/0}$)[c]
Cr	2.38 ± 0.02 (0)[d]	2.51	−0.69 (0)[d]
Mo	2.63 ± 0.02 (+0.25)	2.67	−0.39 (+0.30)
W	2.63 ± 0.01 (+0.25)	2.66	−0.38 (+0.31)

[a]Equivalent to the electron affinity of the radicals $CpM(CO)_3^{\bullet}$. [b]Includes zero-point energy corrections. [c]From ref 17. E° values cited for Mo and W are corrected for the kinetic potential shift. [d]Numbers in parentheses are values relative to the Cr species.

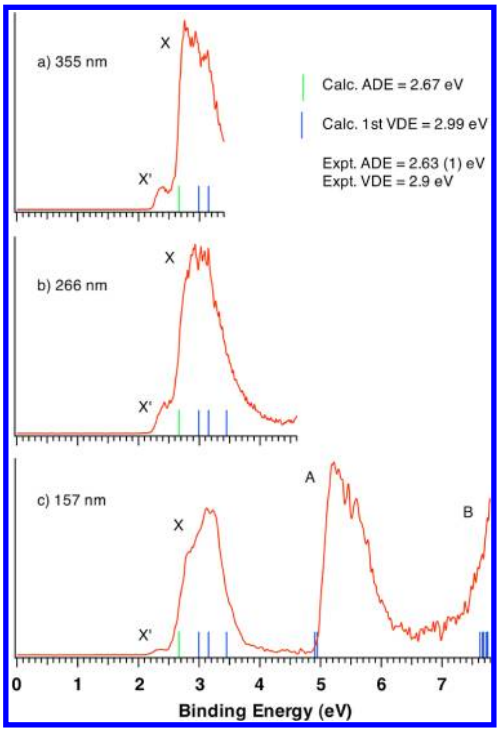

Figure 2. Low-temperature (20 K) photoelectron spectra of $CpMo(CO)_3^-$ at 355 (a), 266 (b), and 157 nm (c). The X′ feature at low binding energy is due to photodetachment of fragment anions (see text for details). The calculated adiabatic (ADE, green bar) and vertical detachment energies (VDEs, blue bars) are indicated.

energy is observed in each spectrum (labeled as X′), and this feature becomes much weaker at 157 nm, whereas it is more readily apparent in the 355 and 266 nm spectra. This weak feature is most likely due to a two-photon process involving photodissociation of $CpMo(CO)_3^-$ (likely loss of CO) followed by photodetachment of a fragment ion, possibly $CpMo(CO)_2^-$. A similar two-photon process of photodetachment and photofragmentation has been observed in experiments on $Mo(CO)_3^{\bullet-}$.[29] We were able to reduce the X′ intensity by decreasing the photon flux but could not completely eliminate this band, presumably due to the photodissociation step being nearly saturated. The ADE is estimated similarly from the rising edge of the main X peak to be 2.63 ± 0.02 eV (Table 1).

The $[CpW(CO)_3]^-$ spectra at 20 K are shown in Figure 3. Similar spectral patterns, with three well-separated features X, A, and B, are revealed at 157 nm. In contrast to both the Cr and Mo anionic species, where a shoulder is marginally discernible

dx.doi.org/10.1021/om3011454 | Organometallics 2013, 32, 2084−2091

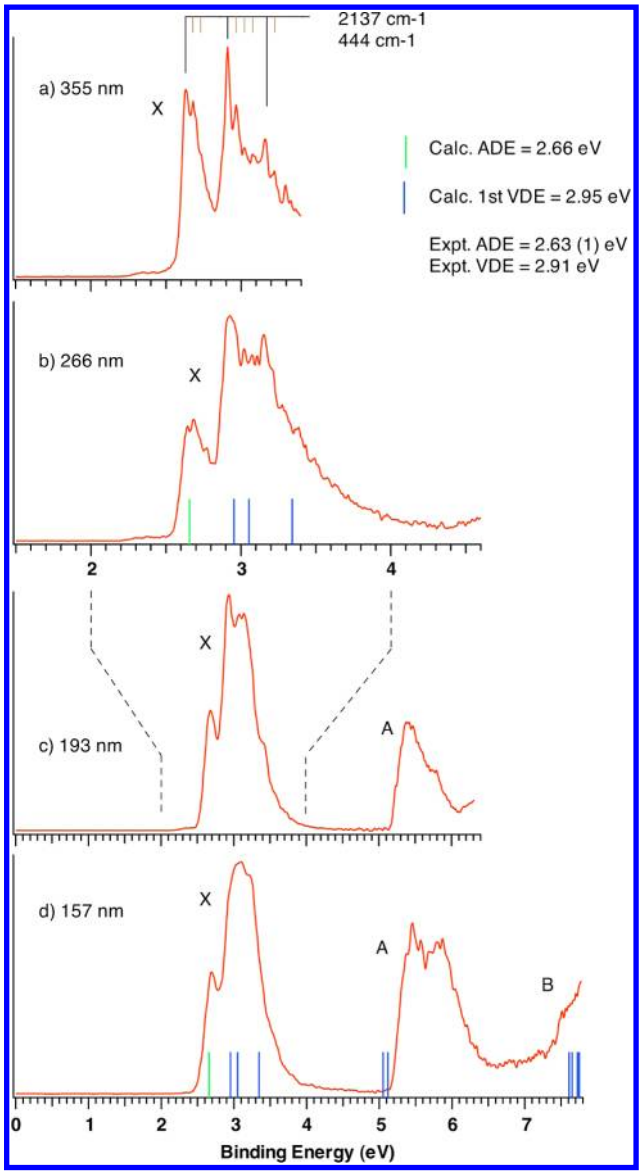

Figure 3. Low-temperature (20 K) photoelectron spectra of $CpW(CO)_3^-$ at 355 (a), 266 (b), 193 (c), and 157 nm (d). Two vibrational progressions are indicated. The calculated adiabatic (ADE, green bar) and vertical detachment energies (VDEs, blue bars) are compared with the spectra.

in the rising edge of the feature X at 157 nm, a relatively sharp peak is resolved at the threshold in the W case. This effect has been observed previously by Lichtenberger and Fenske[24a] in their photoionization study of $CpRe(CO)_3$ vs $CpMn(CO)_3$ and by Lloyd and co-workers in their photoionization study of $W(CO)_6$ vs $Cr(CO)_6$[24c] and is mainly attributed to appreciable spin−orbit interaction for the heavy-metal compounds, resulting in a smaller geometrical variation upon removal of an electron (vide infra). Better resolved spectra were obtained at 193, 266, and 355 nm showing fine spectral features for X (Figure 3c−a) with increasingly improved intrinsic instrumental resolution. Two vibrational progressions with frequencies of 2137 ± 40 and 444 ± 40 cm^{-1} are apparent at 355 nm and are visible at 266 nm. The ADE of $[CpW(CO)_3]^-$, equivalent to the EA of the $CpW(CO)_3^•$ radical, is determined from the first resolved transition to be 2.63 ± 0.01 eV (Table 1). This EA value also serves as a self-calibration by comparison with the method by drawing straight lines along the rising edge to determine the constant that is used to estimate the ADEs for both Cr and Mo species.

A comparison of the 157 nm spectra among the $CpM(CO)_3^-$ (M = Cr, Mo, W) triad (Figure 4) clearly illustrates the

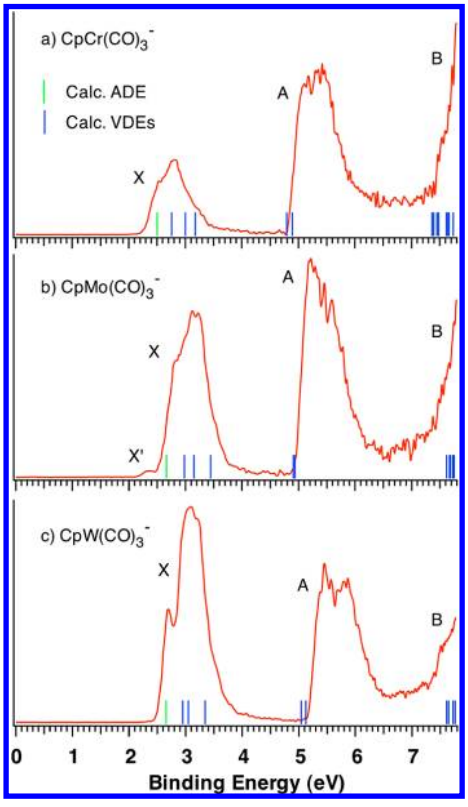

Figure 4. Comparison of 157 nm spectra for the triad $CpM(CO)_3^-$, showing overall similar spectral patterns with increase of the first band intensity along M = Cr (a), Mo (b), and W (c). The calculated adiabatic (ADE, green bar) and vertical detachment energies (VDEs, blue bars) are indicated.

overall similarity in spectral patterns, electron binding energies and band gaps. However, the relative ratio of the two main bands X/A gradually increases from Cr to W. A comparison of the gas-phase EAs and the solution-phase $E°(CpM(CO)_3^{•/-})$ (measured in acetonitrile by cyclic voltammetry)[17] for $CpM(CO)_3^•$ (M = Cr, Mo, W) is presented in Table 1. Within experimental error, it appears that the change of the EAs among the triad tracks the variation of $E°(0/-)$ quite well, although the absolute values are different, as expected.

THEORETICAL RESULTS AND DISCUSSIONS

First-principles calculations were conducted to obtain the optimized geometries of the anions and the neutral radicals, to unravel the structural changes upon photodetaching, to provide an understanding of the electronic structure and chemical bonding of these species, and to compute ADEs and VDEs and excitation energies for direct comparison with the experiments.

Optimized Structures. Figure S1 (Supporting Information) shows the optimized three-legged piano-stool geometries of the $CpM(CO)_3^{-/•}$ pairs, with selected bond lengths and bond angles given in Table 2. Additional metrical data are given in Table S1 (Supporting Information), and atomic coordinates for the DFT-optimized structures are also provided. All M−

dx.doi.org/10.1021/om3011454 | Organometallics 2013, 32, 2084−2091

Table 2. Calculated Bond Lengths (Å) and Bond Angles (deg) for the Optimized Structures of $CpM(CO)_3^{-/\bullet}$ (M = Cr, Mo, W)[a] and Selected Vibrational Frequencies (cm^{-1})

	Cr		Mo		W	
M	anion	neutral	anion	neutral	anion	neutral
			Bond Lengths			
M−C(6)	1.808	1.847	1.949	1.997	1.946	1.969
M−C(7)	1.807	1.859	1.949	1.997	1.947	1.987
M−C(8)	1.807	1.859	1.949	1.975	1.947	1.987
C(6)−O(1)	1.190	1.168	1.190	1.168	1.192	1.170
C(7)−O(2)	1.190	1.167	1.190	1.168	1.192	1.170
C(8)−O(3)	1.191	1.166	1.190	1.168	1.192	1.170
$M-Cp_{centroid}$	1.878	1.864	2.098	2.045	2.071	2.031
			Bond Angles			
C(6)−M−C(7)	91.16	85.50	88.41	99.57	89.27	83.69
C(7)−M−C(8)	91.60	103.40	88.60	83.49	89.58	99.12
C(8)−M−C(6)	90.92	85.73	88.20	83.47	89.37	83.64
			Frequencies (cm^{-1})			
C−O sym stretching	1870	1978	1876	1977	1872	1972
$M-C_{CO}$ sym stretching	507	452	486	469	491	479

[a]Complete bond lengths and angles are given in Table S1 (Supporting Information).

C_{CO} bonds become longer upon electron loss from $CpM(CO)_3^-$, with average elongations of 0.048, 0.041, and 0.034 Å for Cr, Mo, and W, respectively, while all the C−O bonds become shorter by 0.023, 0.022, and 0.022 Å (though all are longer than the free CO bond length of 1.128 Å[41]). These observations are consistent with the HOMO having $M-C_{CO}$ π-bonding character and C−O π^*-antibonding character, as shown in the molecular orbitals (Figure 5). Whereas the three $C_{CO}-M-C_{CO}$ bond angles are essentially the same in the anions, upon electron loss, one of the three $C_{CO}-M-C_{CO}$ bond angles becomes larger (by 11.8, 11.2, and 9.5° for Cr, Mo, and W, respectively), and the other two become smaller (on average by 5.4, 4.9, and 5.6° for Cr, Mo, and W, respectively) due to Jahn−Teller distortion in the 17e neutral radicals.[16]

The M−C−O bond angles are nearly the same for the anions and the neutrals (all ~176−177°). Both the average $M-C_{Cp}$ bond length and $M-Cp_{centroid}$ distance are observed to slightly decrease upon removal of an electron. Overall, the anion-to-neutral structural variation on the $M(CO)_3$ moiety slightly decreases from Cr and Mo to W with RMS deviations of 0.217, 0.222, and 0.206 Å, for Cr, Mo, and W, respectively (see the Supporting Information for details).

Calculated ADEs and VDEs. The ADEs of $CpM(CO)_3^-$ are calculated to be 2.51, 2.67, and 2.66 eV for Cr, Mo, and W, respectively, in good agreement with the experimentally measured values of 2.38, 2.63, and 2.63 eV and the observed ADE trend (Table 1). The calculated VDEs of the anions fit the

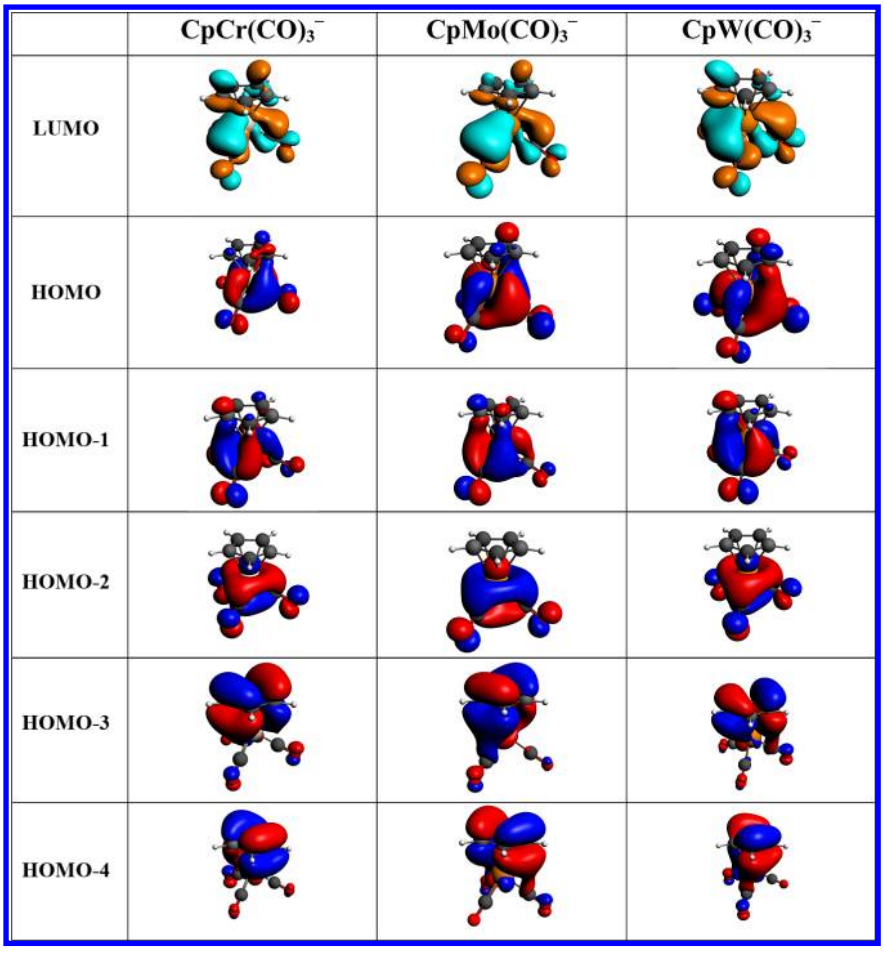

Figure 5. The LUMO and top five occupied molecular orbitals of $CpM(CO)_3^-$. The metal, C, O, and H are in gold, dark gray, red, and light gray, respectively. The spatial representation of the orbitals is shown at an isosurface value of 0.03.

dx.doi.org/10.1021/om3011454 | Organometallics 2013, 32, 2084−2091

maxima of the X bands well, and VDE_{HOMO} is found to be 0.3–0.4 eV larger than the ADE for each anion. This VDE_{HOMO}—ADE difference is caused by the aforementioned appreciable anion–neutral geometrical changes; such relationships between the VDE_{HOMO}–ADE difference and anion–neutral geometrical change have been observed in other systems.[28a,31] The calculated VDEs are shown as sticks in Figures 1–4 (blue bars; the corresponding values are given in Table S3 (Supporting Information)), and are in excellent agreement with the experimental data. The calculations reveal grouped electronic structures for all three neutral species with three, two, and more electronic transitions are involved in the X, A, and B bands, respectively, and clear band gaps between them.

MO and Chemical Bonding Analyses. The LUMO and top five occupied molecular orbitals (MOs) and compositions are shown in Figure 5 and given in Table 3. For each

Table 3. Orbital Energy and Composition for the LUMO and the Top Five Occupied Molecular Orbitals of $CpM(CO)_3^-$ Complexes

MO	*E* (eV)	MO pop. analysis: % M character
	$CpCr(CO)_3^-$	
LUMO	3.196	37
HOMO	−0.097	55
HOMO-1	−0.103	52
HOMO-2	−0.355	57
HOMO-3	−2.475	12
HOMO-4	−2.562	10
	$CpMo(CO)_3^-$	
LUMO	3.026	24
HOMO	−0.330	53
HOMO-1	−0.343	53
HOMO-2	−0.616	59
HOMO-3	−2.591	10
HOMO-4	−2.673	8
	$CpW(CO)_3^-$	
LUMO	3.060	14
HOMO	−0.308	50
HOMO-1	−0.314	51
HOMO-2	−0.545	54
HOMO-3	−2.794	9
HOMO-4	−2.898	9

$CpM(CO)_3^-$ the top three occupied MOs lying close in energy are largely metal-based, followed by an energy gap to the next two MOs. The latter represent the two π bonds between the metal center and C_5H_5. Notably, the σ bonding component of the Cp–M interaction lies more deeply buried (HOMO-18) and is about 6 eV lower in energy than the HOMO. (The side view of a π bond (HOMO-4) and the σ bond (HOMO-18) of $CpW(CO)_3^-$ are shown in Figure S4 (Supporting Information)). The MO scheme is in qualitative agreement with previous theoretical studies using minimum basis sets and MO interaction arguments.[15,20–22] Under the single-particle picture (Koopmans' theorem),[42] the X and A features result from the removal of electrons from the top three metal-based (X) and next two Cp–metal π-bonding MOs (A), respectively. Since the A feature in each species is mainly from the Cp moiety, it is understandable that the A features are similar across the Cr, Mo, and W compounds. Calculations show that the next higher detachment band (B) comes from contributions from many transitions resulting from removal of electrons from deeper bonding orbitals that are nearly degenerate in energy and are mainly involved with the Cp moiety and the CO groups, which is in good agreement with the rising edge of the B feature in each species. The simulated photoelectron stick spectra (Figures 1–4) clearly support the assignments. Ejection of an electron from the Cp–M σ bonding orbital (HOMO-18) occurs at a much higher energy and is out of the range of our experimental measurement. The observed increase of the X/A area ratio down the triad (Figure 4) also agrees with the above analysis, since the metal detachment cross-section (contributing to the X feature) is expected to increase from Cr to Mo to W.[43]

The MO analyses suggest M–C(O) bonding and (M)C–O antibonding interactions, consistent with the calculated anion-to-neutral geometric changes discussed above (i.e., the M–C bond length increases while C–O decreases upon electron detachment). Consequently, we assign the vibrational progression with the frequency of 2137 ± 40 cm^{-1} observed in the X band to the symmetric C–O stretching of the neutral $CpW(CO)_3^•$ species, the observed frequency of which compares reasonably well to the calculated value of 1972 cm^{-1} and reported values from other studies (1999 cm^{-1} measured in heptane by time-resolved IR spectroscopy[12b] and 2000 cm^{-1} in $W(CO)_3$ by PES[29]) . The other vibrational mode of 444 ± 40 cm^{-1} observed in the X band is due to the $W–C_{CO}$ stretching mode, in good agreement with the reported value of 480 cm^{-1} of $[CpW(CO)_3]_2$[44] and the calculated frequency of 479 cm^{-1}. The apparently better resolved spectra for the W species among the triad is at least partially due to the fact that the OC–M–CO bond angle distortion, which is associated with very low frequency modes and tends to smear out other vibrational structures, is lowest for the W species.

Comparison of the Bond Strengths between Cp and $M(CO)_3$ in the $CpM(CO)_3^{-/•}$ Triad. Previous negative ion PES studies reported the EAs of $M(CO)_3$ to be 1.349, 1.337, and 1.859 eV for M = Cr, Mo, W, respectively,[29] and the EA of $Cp^•$ to be 1.786 eV.[45] Consequently, the $[Cp\cdots M(CO)_3]^-$ dissociation likely leads to the charge remaining on the Cp fragment. Therefore, we can estimate the bond dissociation energy differences of Cp and $M(CO)_3$ moieties in anionic and neutral states according to eqs 1–3, and by using the

$$D_0[CpM(CO)_3] = E_0[M(CO)_3] + E_0(Cp) - E_0[CpM(CO)_3] \quad (1)$$

$$D_0[CpM(CO)_3^-] = E_0[M(CO)_3] + E_0(Cp^-) - E_0[CpM(CO)_3^-] \quad (2)$$

$$\Delta D_0 = D_0[CpM(CO)_3^-] - D_0[CpM(CO)_3] = EA[CpM(CO)_3] - EA[Cp] \quad (3)$$

experimental EA values obtained in this work, to be 0.59, 0.84, and 0.84 eV for Cr, Mo, and W, respectively. The rough estimates suggest that the bonding between Cp^- and $M(CO)_3$ is stronger than that between $Cp^•$ and $M(CO)_3$, and the increased bond strength increases from the first-row metal to the second and third rows.

dx.doi.org/10.1021/om3011454 | *Organometallics* 2013, 32, 2084–2091

PERSPECTIVE AND CONCLUSION

Electron affinities, reduction potentials, and energies of lowest empty (or partially filled) MOs are crucial for understanding virtually all chemical reactions and catalytic processes involving electron transfers. They are interconnected and often correlated but are defined in the gas phase and solution and by theory, respectively. Open-shell metal-centered radicals are highly reactive species and are generally only observed as transient reaction intermediates; consequently, solution-phase measurement of molecular properties, such as reliable redox potentials, is challenging. By taking advantage of the stability of the corresponding closed-shell anions in solutions, we can "fish out" these anions from solutions via ESI and probe their electronic structures in the gas phase. The obtained ground and excited state information, and electron affinities of the neutral radicals, can be compared directly with theoretical calculations. In this paper, a joint experimental−theoretical study was carried out to analyze electronic and geometrical structures of 17e $CpM(CO)_3^{\bullet}$ radicals. Photoelectron spectra reveal similar spectral patterns with band gaps, and hence electronic structures, for the neutral triad. The EA of $CpM(CO)_3^{\bullet}$ is determined to be 2.38 eV for the Cr and 2.63 eV for both Mo and W species, with this trend being in excellent accord with the redox potentials measured in solution. Theoretical computations show the piano-stool structure for all anions and neutral radicals, with electronic states grouped with clear separations, in excellent agreement with the experimental photoelectron spectra. In addition, the subsequent MO and chemical bonding analyses quantify the MO interaction scheme, in which the top three filled MOs lying close in energy contain more than 50% contribution from the metal, followed by an energy gap and two metal−Cp π bonding MOs. Experimental data show stronger bonding interactions between Cp and $M(CO)_3$ in the anionic than in the neutral forms and an increasing trend of such interaction differences from Cr to Mo and W. The intrinsic energetic and structural information obtained in this study, including excited states, can help explain and understand fundamental reactivity patterns for this class of organometallic complexes.

ASSOCIATED CONTENT

Supporting Information

Text, tables, and figures giving details of determining the ADE from the photoelectron spectra, metrical parameters, coordinates, and plots of the optimized structures of $CpM(CO)_3^{-/\bullet}$, energies of selected MOs of $CpM(CO)_3^{\bullet}$, calculated VDEs, and selected additional MO plots of $CpW(CO)_3^{\bullet}$. This material is available free of charge via the Internet at http://pubs.acs.org.

AUTHOR INFORMATION

Corresponding Author

*E-mail: X.-B.W., xuebin.wang@pnnl.gov; P.Y., ping.yang@pnnl.gov; R.M.B., morris.bullock@pnnl.gov.

Present Address

[§]Visiting student. Present address: State Key Laboratory of Molecular Reaction Dynamics, Institute of Chemistry, Chinese Academy of Sciences, Beijing 100190, People's Republic of China (G.-L.H.); Laboratory of Atmospheric Physical Chemistry, Anhui Institute of Optics & Fine Mechanics, Chinese Academy of Sciences, Hefei, Anhui 230031, People's Republic of China (H.W.).

Notes

The authors declare no competing financial interest.

ACKNOWLEDGMENTS

We thank the reviewers for very helpful comments and suggestions. This work was supported by the U.S. Department of Energy, Office of Science, Office of Basic Energy Sciences, Division of Chemical Sciences, Geosciences and Biosciences. P.Y. acknowledges partial support from the Environmental Molecular Sciences Laboratory (EMSL) through its intramural program. A portion of the research was performed using EMSL, a national scientific user facility sponsored by the Department of Energy's Office of Biological and Environmental Research and located at Pacific Northwest National Laboratory (PNNL). Pacific Northwest National Laboratory is operated by Battelle for the U.S. Department of Energy.

REFERENCES

(1) Baird, M. C. *Chem. Rev.* **1988**, *88*, 1217−1227.
(2) Tyler, D. R. *Acc. Chem. Res.* **1991**, *24*, 325−331.
(3) McLain, S. J. *J. Am. Chem. Soc.* **1988**, *110*, 643−644.
(4) Meyer, T. J.; Caspar, J. V. *Chem. Rev.* **1985**, *85*, 187−218.
(5) Scott, S. L.; Espenson, J. H.; Zhu, Z. *J. Am. Chem. Soc.* **1993**, *115*, 1789−1797.
(6) VanVlierberge, B. A.; Abrahamson, H. B. *J. Photochem. Photobiol. A: Chem.* **1990**, *52*, 69−81.
(7) Yao, Q.; Bakac, A.; Espenson, J. H. *Organometallics* **1993**, *12*, 2010−2012.
(8) Watkins, W. C.; Jaeger, T.; Kidd, C. E.; Fortier, S.; Baird, M. C.; Kiss, G.; Roper, G. C.; Hoff, C. D. *J. Am. Chem. Soc.* **1992**, *114*, 907−914.
(9) (a) Tanner, P. S.; Barbini, D. C.; Jones, W. E., Jr. *Inorg. Chem.* **1997**, *36*, 6457−6460. (b) Wittrig, R. E.; Kubiak, C. P. *J. Electroanal. Chem.* **1995**, *393*, 75−86.
(10) (a) Moss, J. R. *Trends Organomet. Chem.* **1994**, *1*, 211. (b) Yin, X.; Moss, J. R. *J. Organomet. Chem.* **1999**, *574*, 252−266. (c) Tang, L.; Norton, J. R. *Macromolecules* **2006**, *39*, 8236−8240. (d) Choi, J.; Tang, L.; Norton, J. R. *J. Am. Chem. Soc.* **2007**, *129*, 234−240.
(11) (a) Scott, S. L.; Espenson, J. H.; Chen, W. J. *Organometallics* **1993**, *12*, 4077−4084. (b) Trogler, W. C., Ed. *Organometallic Radical Processes*; Elsevier: New York, 1990; p 22.
(12) (a) Peters, J.; George, M. W.; Turner, J. J. *Organometallics* **1995**, *14*, 1503−1506. (b) Virrels, I. G.; George, M. W.; Johnson, F. P. A.; Turner, J. J.; Westwell, J. R. *Organometallics* **1995**, *14*, 5203−5208.
(13) (a) Stiegman, A. E.; Stieglitz, M.; Tyler, D. R. *J. Am. Chem. Soc.* **1983**, *105*, 6032−6037. (b) Stiegman, A. E.; Tyler, D. R. *Coord. Chem. Rev.* **1985**, *63*, 217−240. (c) Scott, S. L.; Espenson, J. H.; Bakac, A. *Organometallics* **1993**, *12*, 1044−1047. (d) Song, J.-S.; Bullock, R. M.; Creutz, C. *J. Am. Chem. Soc.* **1991**, *113*, 9862−9864.
(14) (a) Cahoon, J. F.; Kling, M. F.; Schmatz, S.; Harris, C. B. *J. Am. Chem. Soc.* **2005**, *127*, 12555−12565. (b) Cahoon, J. F.; Kling, M. F.; Sawyer, K. R.; Frei, H.; Harris, C. B. *J. Am. Chem. Soc.* **2006**, *128*, 3152−3153. (c) Sawyer, K. R.; Cahoon, J. F.; Shanoski, J. E.; Glascoe, E. A.; Matthias, F. K.; Schlegel, J. P.; Zoerb, M. C.; Hapke, M.; Hartwig, J. F.; Webster, C. E.; Harris, C. B. *J. Am. Chem. Soc.* **2010**, *132*, 1848−1859. (d) Glascoe, E. A.; Kling, M. F.; Shanoski, J. E.; DiStasio, R. A., Jr.; Payne, C. K.; Mork, B. V.; Tilley, T. D.; Harris, C. B. *Organometallics* **2007**, *26*, 1424−1432. (e) Kling, M. F.; Cahoon, J. F.; Glascoe, E. A.; Shanoski, J. E.; Harris, C. B. *J. Am. Chem. Soc.* **2004**, *126*, 11414−11415.
(15) Woska, D. C.; Ni, Y. P.; Wayland, B. B. *Inorg. Chem.* **1999**, *38*, 4135−4138.
(16) Fortier, S.; Baird, M. C.; K., F.; Morton, J. R.; Ziegler, T.; Jaeger, T. J.; Watkins, W. C.; MacNeil, J. H.; Watson, K. A.; Hensel, K.; Page, Y. L.; Charland, J. P.; Williams, A. J. *J. Am. Chem. Soc.* **1991**, *113*, 542−551.

(17) (a) Tilset, M.; Parker, V. D. *J. Am. Chem. Soc.* **1989**, *111*, 6711−6717; as modified in *J. Am. Chem. Soc.* **1990**, *112*, 2843. (b) Kadish, K. M.; Lacombe, D. A.; Anderson, J. E. *Inorg. Chem.* **1986**, *25*, 2246−2250.
(18) Watkins, W. C.; Jaeger, T. J.; Kidd, C. E.; Fortier, S.; Baird, M. C.; Kiss, G.; Roper, G. C.; Hoff, C. D. *J. Am. Chem. Soc.* **1992**, *114*, 907−914.
(19) (a) Roberts, J. A. S.; Franz, J. A.; van der Eide, E. F.; Walter, E. D.; Petersen, J. L.; DuBois, D. L.; Bullock, R. M. *J. Am. Chem. Soc.* **2011**, *133*, 14593−14603. (b) Roberts, J. A. S.; Appel, A. M.; DuBois, D. L.; Bullock, R. M. *J. Am. Chem. Soc.* **2011**, *133*, 14604−14613. (c) Roberts, J. A. S.; DuBois, D. L.; Bullock, R. M. *Organometallics* **2011**, *30*, 4555−4563. (d) van der Eide, E. F.; Liu, T. B.; Camaioni, D. M.; Walter, E. D.; Bullock, R. M. *Organometallics* **2012**, *31*, 1775−1789. (e) van der Eide, E. F.; Helm, M. L.; Walter, E. D.; Bullock, R. M. *Inorg. Chem.* **2013**, *52*, 1591−1603.
(20) (a) Hoffmann, R. *Science* **1981**, *211*, 995−1002. (b) Albright, T. A.; Hofmann, P.; Hoffmann, R. *J. Am. Chem. Soc.* **1977**, *99*, 7546−7557.
(21) (a) Elian, M.; Chen, M. M. L.; Mingos, D. M. P.; Hoffmann, R. *Inorg. Chem.* **1976**, *15*, 1148−1155. (b) Elian, M.; Hoffmann, R. *Inorg. Chem.* **1975**, *14*, 1058−1076.
(22) Veiros, L. F. *Organometallics* **2000**, *19*, 5549−5558.
(23) (a) Byers, B. P.; Hall, M. B. *Organometallics* **1987**, *6*, 2319−2325. (b) Low, A. A.; Hall, M. B. *Int. J. Quantum Chem.* **2000**, *77*, 152−160. (c) Lin, Z. Y.; Hall, M. B. *Organometallics* **1993**, *12*, 19−23.
(24) (a) Lichtenberger, D. L.; Fenske, R. F. *J. Am. Chem. Soc.* **1976**, *98*, 50−63. (b) Asirvatham, V. S.; Gruhn, N. E.; Lichtenberger, D. L.; Ashby, M. T. *Organometallics* **2000**, *19*, 2215−2227. (c) Higginson, B. R.; Lloyd, D. R.; Burroughs, P.; Gibson, D. M.; Orchard, A. F. *J. Chem. Soc., Faraday Trans. 2* **1973**, *69*, 1659−1668.
(25) Green, J. C.; Jackson, S. E. *J. Chem. Soc., Dalton Trans.* **1976**, 1698−1702.
(26) Rienstra-Kiracofe, J. C.; Tschumper, G. S.; Schaefer, H. F.; Nandi, S.; Ellison, G. B. *Chem. Rev.* **2002**, *102*, 231−282.
(27) (a) Wang, X. B.; Wang, L. S. *J. Am. Chem. Soc.* **2000**, *122*, 2339−2345. (b) Waters, T.; Wang, X. B.; Wang, L. S. *Coord. Chem. Rev.* **2007**, *251*, 474−491.
(28) (a) Wang, X. B.; Wang, Y. L.; Yang, J.; Xing, X. P.; Li, J.; Wang, L. S. *J. Am. Chem. Soc.* **2009**, *131*, 16368−16369. (b) Hou, G. L.; Wen, H.; Lopata, K.; Zheng, W. J.; Kowalski, K.; Govind, N.; Wang, X. B.; Xantheas, S. S. *Angew. Chem., Int. Ed.* **2012**, *51*, 6356−6360.
(29) Bengali, A. A.; Casey, S. M.; Cheng, C. L.; Dick, J. P.; Fenn, P. T.; Villalta, P. W.; Leopold, D. G. *J. Am. Chem. Soc.* **1992**, *114*, 5257−5268.
(30) (a) Birdwhistell, R.; Hackett, P.; Manning, A. R. *J. Organomet. Chem.* **1978**, *157*, 239−241. (b) Tate, D. P.; Knipple, W. R.; Augl, J. M. *Inorg. Chem.* **1962**, *1*, 433−434. (c) Smart, J. C.; Curtis, C. J. *Inorg. Chem.* **1977**, *16*, 1788−1790. (d) Behrens, U.; Edelmann, F. *J. Organomet. Chem.* **1984**, *263*, 179.
(31) Wang, X. B.; Wang, L. S. *Rev. Sci. Instrum.* **2008**, *79*, 073108.
(32) Gilles, M. K.; Polak, M. L.; Lineberger, W. C. *J. Chem. Phys.* **1992**, *96*, 8012−8020.
(33) Perdew, J. P.; Burke, K.; Ernzerhof, M. *Phys. Rev. Lett.* **1996**, *77*, 3865−3868.
(34) (a) te Velde, G.; Bickelhaupt, F. M.; Baerends, E. J.; Guerra, C. F.; Van Gisbergen, S. J. A.; Snijders, J. G.; Ziegler, T. *J. Comput. Chem.* **2001**, *22*, 931−967. (b) Guerra, C. F.; Snijders, J. G.; te Velde, G.; Baerends, E. *J. Theor. Chem. Acc.* **1998**, *99*, 391−403 (ADF2010; SCM, Theoretical Chemistry, Vrije Universiteit, Amsterdam, The Netherlands).
(35) van Lenthe, E.; Baerends, E. J. *J. Comput. Chem.* **2003**, *24*, 1142−1156.
(36) van Lenthe, E.; Baerends, E. J.; Snijders, J. G. *J. Chem. Phys.* **1993**, *99*, 4597−4610.
(37) (a) Bérces, A.; Dickson, R. M.; Fan, L. Y.; Jacobsen, H.; Swerhone, D.; Ziegler, T. *Comput. Phys. Commun.* **1997**, *100*, 247−262. (b) Wolff, S. K. *Int. J. Quantum Chem.* **2005**, *104*, 645−659.
(38) Gross, E. K. U.; Dobson, J. F.; Petersilka, M. In *Topics in Current Chemistry: Density Functional Theory II*; Nalewajski, R. F., Ed.; Springer: Berlin, 1996; Vol. *181*, pp 81−172.
(39) Li, J.; Li, X.; Zhai, H. J.; Wang, L. S. *Science* **2003**, *299*, 864−867.
(40) Wang, Y. L.; Zhai, H. J.; Xu, L.; Li, J.; Wang, L. S. *J. Phys. Chem. A* **2010**, *114*, 1247−1254.
(41) NIST Chemistry Webbook. http://webbook.nist.gov (Nov 2012).
(42) Koopmans, T. *Physica* **1934**, *1*, 104−113.
(43) (a) Mandl, A. *Phys. Rev. A* **1976**, *14*, 345−348. (b) Covington, A. M.; Duvvuri, S. S.; Emmons, E. D.; Kraus, R. G.; Williams, W. W.; Thompson, J. S.; Calabrese, D.; Carpenter, D. L.; Collier, R. D.; Kvale, T. J.; Davis, V. T. *Phys. Rev. A* **2007**, *75*, 022711.
(44) Parker, D. J. *J. Chem. Soc. A* **1970**, 1382−1386.
(45) Engelking, P. C.; Lineberger, W. C. *J. Chem. Phys.* **1977**, *67*, 1412−1417.